

GRAVITY RECOVERY AND INTERIOR LABORATORY MISSION (GRAIL) ORBIT DETERMINATION

**Tung-Han You⁽¹⁾, Peter Antreasian⁽²⁾, Stephen Broschart⁽³⁾, Kevin Criddle⁽⁴⁾ Earl Higa⁽⁵⁾,
David Jefferson⁽⁶⁾, Eunice Lau⁽⁷⁾, Swati Mohan⁽⁸⁾, Mark Ryne⁽⁹⁾, Mason Keck⁽¹⁰⁾**

⁽¹⁾⁻⁽⁹⁾ Jet Propulsion Laboratory, California Institute of Technology, 4800 Oak Grove Drive, Pasadena, CA 91109
+1-818-354-5745, {Tung-Han.You, Peter.G.Antreasian, Stephen.B.Broschart, Kevin.E.Criddle, Earl.S.Higa,
David.C.Jefferson, Eunice.K.Lau, Swati.Mohan, Mark.S.Ryne}@jpl.nasa.gov

⁽¹⁰⁾ Dept. of Astronomy, Boston University, 725 Commonwealth Ave., Boston, MA 02215, Mason.Keck@gmail.com

Abstract: Launched on 10 September 2011 from the Cape Canaveral Air Force Station, Florida, the twin-spacecraft Gravity Recovery and Interior Laboratory (GRAIL) has the primary mission objective of generating a lunar gravity map with an unprecedented resolution via the Ka-band Lunar Gravity Ranging System (LGRS). After successfully executing nearly 30 maneuvers on their six-month journey, Ebb and Flow (aka GRAIL-A and GRAIL-B) established the most stringent planetary formation orbit on 1 March 2012 of approximately 30 km x 90 km in orbit size. This paper describes the orbit determination (OD) filter configurations, analyses, and results during the Trans-Lunar Cruise, Orbit Period Reduction, and Transition to Science Formation phases. The maneuver reconstruction strategies and their performance will also be discussed, as well as the navigation requirements, major dynamic models, and navigation challenges. GRAIL is the first mission to generate a full high-resolution gravity field of the only natural satellite of the Earth. It not only enables scientists to understand the detailed structure of the Moon but also further extends their knowledge of the evolutionary histories of the rocky inner planets. Robust and successful navigation was the key to making this a reality.

Keywords: GRAIL, Orbit Determination, Formation Flying, Navigation, Ebb, Flow, TLC, LOI, OPR, TSF.

1. Introduction

The twin GRAIL spacecraft, Ebb and Flow (aka GRAIL-A and GRAIL-B), were launched on 10 September 2011 at the Cape Canaveral Air Force Station, Florida. The mission's primary objective is to generate the lunar gravity map with an unprecedented resolution via the Ka-band Lunar Gravity Ranging System (LGRS). This will help scientists to characterize the Moon's internal core structure and its thermal history. In addition to the Ka-band Lunar Gravity Ranging System (LGRS) payload, each GRAIL spacecraft (S/C) also carries the MoonKAM lunar-imaging system for educational purposes.

GRAIL adopted a low-energy lunar-transfer trajectory design, which saved more than 100 m/s of the mission ΔV compared to a direct lunar-transfer approach [1] [2]. GRAIL consists of seven mission phases: Launch, Trans-Lunar Cruise (TLC), Lunar Orbit Insertion (LOI), Orbit Period Reduction (OPR), Transition to Science Formation (TSF), Science, and Decommissioning Phases. Figure 1 shows the heliocentric view of the GRAIL Primary Mission phases.

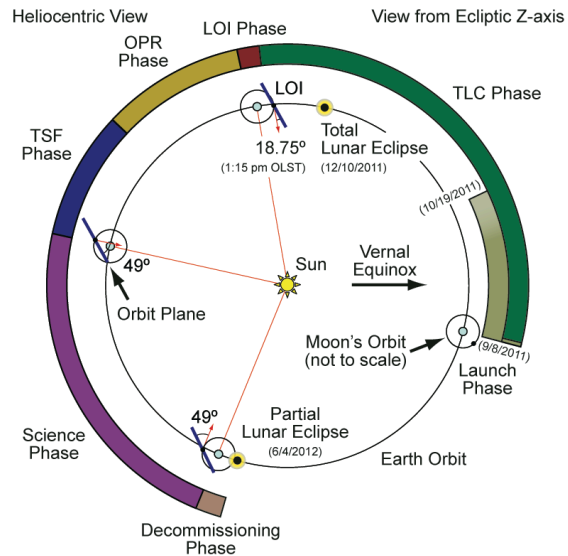


Figure 1: GRAIL Mission Phases

In contrast to most missions that typically have a 3-week launch opportunity, GRAIL had a pretty lengthy launch period of 6 weeks from 08 September 2011 to 19 October 2011. Each launch window consisted of two daily instantaneous launch opportunities with two azimuths, 93° and 99° , separated by about 40 minutes. The launch geometry was nearly invariant.

Shortly after liftoff onboard the Delta II 7920H-10C (see Figure 2), GRAIL was in-view from the Tracking and Data Relay Satellite System (TDRSS) for telemetry relay. Approximately eighty minutes after liftoff, the Goldstone complex of the Deep Space Network (DSN) acquired downlink signals. Sixty minutes after that, two-way tracking data were acquired. The orbit determination (OD) teams delivered their first OD solutions at about seven hours after launch. These solutions enabled the successful signal acquisition of GRAIL-A and B at the subsequent DSN stations at Canberra complex in Australia. Refined launch OD solutions were also mapped back to the Target Interface Point (TIP) to assess the launch vehicle performance in terms of Earth-relative target parameters. The results indicated they were within 0.4σ of expected values.



Figure 2: Ebb and Flow Launched by Delta II

Five Trans-Lunar Cruise (TLC) Trajectory Correction Maneuvers (TCMs) were planned for each spacecraft to satisfy the Lunar Orbit Insertion (LOI) targets. Two were deterministic maneuvers and three were statistical maneuvers. To establish the science formation orbit, excluding the LOI-A and LOI-B maneuvers, there were 9 additional maneuvers for GRAIL-A and 10 additional maneuvers for GRAIL-B performed in the OPR and TSF phases. Figure 3 illustrates Trans-Lunar Cruise, LOI, and OPR trajectories. It also shows the deterministic maneuver locations relative to the Sun-Earth Lagrange Point 1 (EL_1).

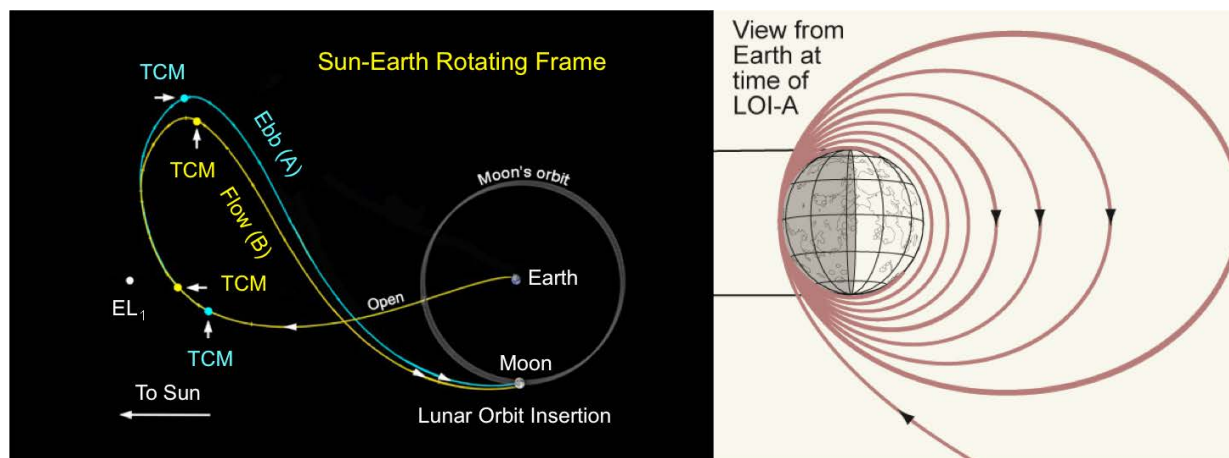


Figure 3: GRAIL Low-energy TLC, LOI, and OPR Trajectories

This paper describes GRAIL orbit determination prior to the Science Phase. It summarizes OD filter configurations, analyses, and results during the TLC, OPR, and TSF phases. The maneuver reconstruction strategies and their performance are also discussed, as well as the navigation requirements, major dynamic models, and challenges.

2. Navigation Requirements and Spacecraft Systems

2.1. Major Navigation Requirements

Navigation was required to provide trajectories to support the launch initial acquisition. Continuous operation was necessary through launch plus 16 hours. Performing quick turn-around solutions was critical in generating launch trajectory updates for the initial and subsequent acquisitions. Extensive preparation and risk reduction efforts were dedicated to this critical period.

GRAIL was also required to satisfy stringent formation requirements at the start of the Science Phase, such as spacecraft-to-spacecraft pointing within $\pm 0.1^\circ$, orbit plane matching within $\pm 0.02^\circ$, separation distance in the range of 50km - 250km, etc¹.

2.2. Challenges

The trajectory designs to ultimately establish the formation orbit required a total of 32 maneuvers (excluded maneuvers during the Science Phase). The drivers for this strategy included the following:

- a. Non-hyperbolic Orbit Insertion: The trans-lunar orbits were not hyperbolic trajectories that typically were seen on flybys or orbit-insertion missions (e.g. Stardust-NExT Tempel-1 flyby, Mars Orbit Insertions). The B-plane targeting paradigm could not be used for these trajectories. To evaluate the consistency of the navigation solutions, a special pseudo B-plane coordinate system was created.
- b. Complex Contingency Scenarios: Since the majority of the maneuvers were deterministic burns, missing some of the key ones would be catastrophic in terms of meeting the mission's success criteria. To better guide the flight operation in dealing with various contingency situations, the GRAIL Mission Design (MD) team published a preliminary version of the "GRAIL Contingency Playbook" pre-launch. However, owing to its complexity and time consuming in analyzing all possible cases, the MD team decided not to release a final version. Instead, the scenarios were continually updated during flight. More than 330 different contingency scenarios were investigated. It eventually required nearly a half-year of computer time to complete these scenarios.
- c. Limited Resolution on Farside Lunar Gravity: The pre-launch best gravity field available to the navigation team was significantly limited in quality on the backside. This weakness was not improved until the GRAIL Gravity Team released an internal version of lunar gravity field solely based on LGRS ka-band data in the middle of the Primary Science Phase. Poor understanding of the backside gravity was a dominant factor in obtaining consistent solutions in some earlier cases. During some parts of the orbital phases, it was deemed necessary to deploy a short-arc strategy to minimize its impact.

2.3. Spacecraft Coordinate Frame and Key Subsystems

The Ebb and Flow spacecraft share exactly the same hardware set. The only differences are in the configuration setup for the LGRS, star tracker, and MoonKAM to support the spacecraft-to-spacecraft pointing orientation in the Science Phase. The spacecraft dry weight is about 200kg and it carried about 106 kg worth of propellant per vehicle.

Each spacecraft consists of one structural subsystem (bus) and two solar arrays. To shield and protect the flight sub-systems, the solar-array side of the bus panel extends 70% wider than its main body. Figure 4 shows the GRAIL spacecraft configuration.

2.3.1 S/C Coordinate System

Ebb and Flow have the exact same definition of the spacecraft body-fixed frame. As shown in Figure 4, the S/C body-fixed +X-axis is along the centerline of propellant tank and main engine thrust direction, the S/C +Y-axis is along the left-front-side solar array, and the S/C +Z-axis is completed by the right-hand rule. The origin is centered on the Y-Z plane and located on the -X bus surface.

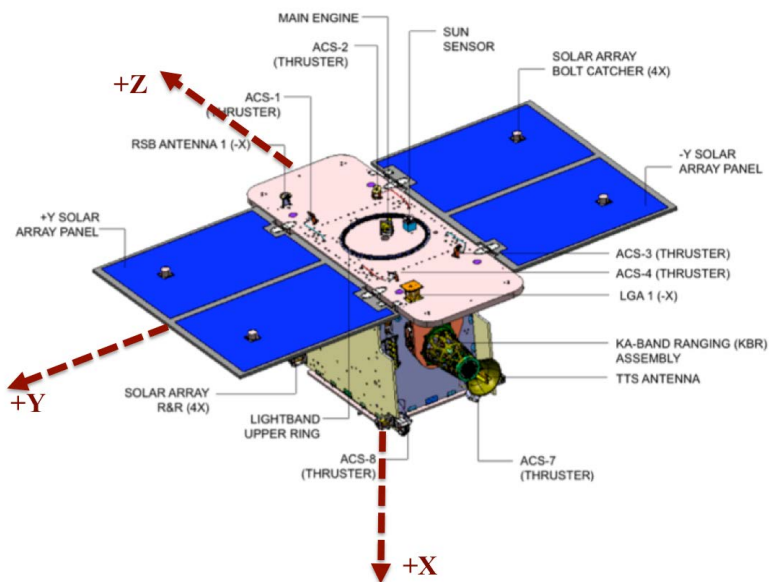


Figure 4: GRAIL Spacecraft Configuration

2.3.2 Propulsion & ACS

GRAIL has a three-axis stabilized Attitude Control System (ACS) relying on star tracker, Sun sensor, Reaction Wheel Assembly (RWA), and Inertial Measurement Unit (IMU) to control the spacecraft attitude. The main engine is mounted along the S/C -X panel. The thrust direction is applied along

the S/C +X axis. There are 4 pairs of balanced thrusters canted 15° and 35° from the X-axis in the X-Z and X-Y planes respectively. The cant-angle design and configuration warrant that these thrusters not only can be used as a balanced system for RWA desaturations but also for small maneuver applications, that is, with selected thruster pairs, it can generate translational ΔV along the $\pm Z$ axes while ΔV s along the other axes are cancelled. This is very useful when small maneuvers are needed. Table 1 summarizes the thruster specifications. The MR-106 main engine was used for TCMs, Period Reduction Maneuvers (PRM), and Transition to Science formation phase Maneuvers (TSM). The Lockheed Martin Corporation proprietary Warm Gas ACS subsystem was used for reaction wheel desaturations and small-size maneuvers such as Orbit Trim Maneuver (OTM).

Table 1: Thruster Types and Specification

Specification	Thrust (N)	Number	Use
Main Engine MR-106	22.0	1	TCMs, PRM, TSM, LOI
Warm Gas ACS Thruster	0.9	8	Attitude Control, Desaturation, Small-size maneuvers

The main engine utilizes a blow-down hydrazine system with a multiple recharging capability. To maintain the thruster performance, the propellant tank was repressurized twice during the flight operation, (once before and once after LOI). Expected thrust performance was provided prelaunch by the spacecraft team for navigation analyses and modeling. As the tank pressure dropped, the thrust performance got degraded. After the completion of the OPR cluster maneuvers, the thrust output roughly reduced to a 50% level from its peak, that is, to generate the same ΔV capability, it would take more than double the on-time [3]

Since the thrust output level varied during maneuver execution, a 6-degree polynomial thrust function was provided by the spacecraft team prior to each maneuver design. The implemented design then was incorporated in the OD process for maneuver reconstruction and orbit propagation.

2.3.3 Telecommunication System

Two Low Gain Antennas (LGA) are mounted on the $\pm X$ sides for each spacecraft. The on-board S-band transponder is capable of generating two-way coherent S-band Doppler and range data, which are the main data types for the orbit determination process. The +X LGA was used during the TLC phase and alternate between the two LGAs during orbital phases. In addition to the S-band transponder, there are also two X-band Radio Science Beacons (RSB) mounted on the $\pm X$ faces with an Ultra-Stable Oscillator (USO), which are capable of generating highly stabilized one-way X-band Doppler data.

3. Spacecraft Dynamic Models

Major forces influencing the GRAIL flight path are gravity, solar radiation pressure, thruster events, and outgassing. Excluding maneuver execution errors, the solar pressure, outgassing events, and thermal imbalance were the major dynamic error sources in the cruise phase, while the lunar gravity uncertainty

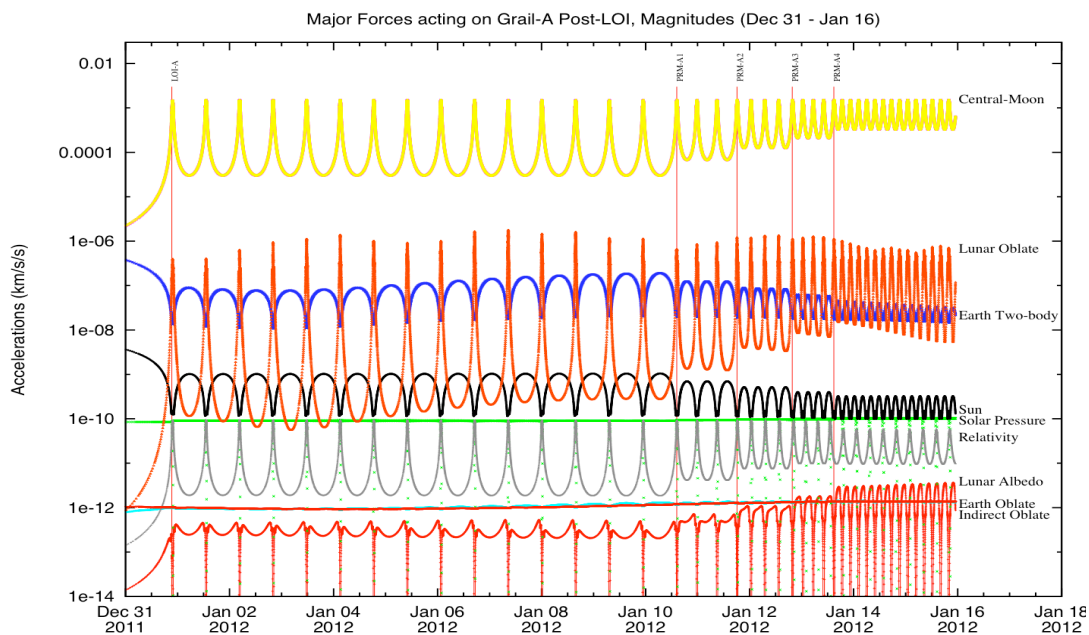


Figure 5: Major Forces Acting on GRAIL, Post-LOI Orbit

was the largest error contributor in the orbital phases. Figure 5 illustrates a pre-launch analysis of the major forces acting on GRAIL post-LOI. Lunar albedo and the Earth oblate gravity field are insignificant ($\sim 10^{-12}$ km/s²) compared with other forces.

Solar radiation pressure was the dominant non-gravitational force during the TLC phase. To improve this model, solar pressure calibration activities were conducted during the mid-cruise phase. Other non-gravitational forces such as outgassing due to the evaporation of residual substance and small forces induced by momentum desaturation events were also investigated. To characterize the small force behavior, one active thruster calibration was performed on each spacecraft. In the orbit phase, the lunar gravity mismodeling becomes the dominant error source. An updated OD filter strategy was introduced to reduce the gravity signature while also improving the spacecraft ephemeris predictability.

3.1. Spacecraft Orientation

Accurate spacecraft orientation is essential to minimize the solar radiation pressure error. It also helped the navigation team to perform trending analyses on small force errors and unmodeled accelerations. The small-force errors were due to imperfections in ACS thruster alignments or/and its control system. The forces typically were projected and estimated in the S/C body-fixed frame for better characterizing the root causes of the errors. The navigation team modeled the spacecraft orientation changes via quaternion representations. Reconstructed quaternions were updated once per week on top of a default background attitude profile³.

For the majority of the cruise, the spacecraft was at the Sun-pointing attitude (i.e. the S/C –X-axis pointed to the Sun). During the solar radiation calibration, the spacecraft was $\pm 45^\circ$ off-pointed from the Sun. A constant 40° off Sun-pointing from the S/C –X-axis was maintained during the OPR and TSF phases. Figure 6 demonstrates the schematic of the attitude configuration during OPR and TSF phases.

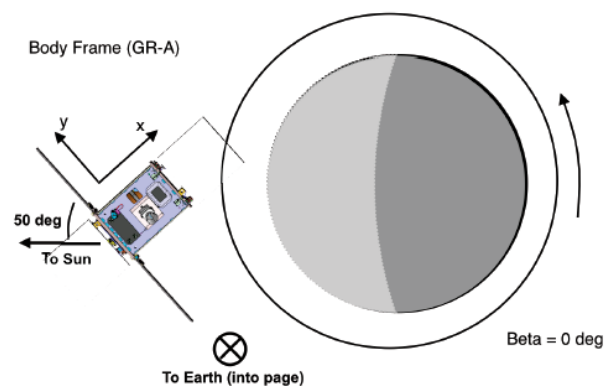


Figure 6: S/C Attitude during OPR/TSF Phases

3.2. Gravity Models

A truncated version of the Earth gravity model based on the GRACE mission [4] was used throughout the GRAIL mission phases. The JPL LP150Q [5] full-field oblateness model was used during the orbital phases. The major contributor in generating this field was NASA's third Discovery mission, Lunar Prospector (LP). Even though it contains high-resolution gravity coverage of the entire nearside, its farside determination is still very weak. This posed a great challenge for navigation in fitting the low orbit data during the orbital phases. Starting from the second half of the Science Phase, a global high-resolution gravity field was obtained. It was solely generated based on the GRAIL LGRS data by the JPL GRAIL Lunar Gravity team. Several internal versions were released thereafter for modeling improvement.

Newtonian point masses for the Sun, and other planets with an additional relativistic influence calculated for the Sun were accounted for the gravitational force as well. JPL DE421 [6] was used for the planetary ephemerides and constants. At the time of GRAIL's Lunar Orbit Insertions, the associated lunar position uncertainty is about 4 m (1σ).

3.3. Solar Radiation Pressure Model

The physical structure of GRAIL was decomposed into 8 representative components for solar radiation computation. Six single sided flat plates represented the six faces of the bus; two single sided flat plates modeled the solar array front and back. The components were fixed with respect to the spacecraft body and no gimbaling drivers. Each plate was assigned diffusive and specular coefficients, which were derived from the associated reflectivity and component properties. From lessons learned on Mars Reconnaissance Orbiter, the solar array diffusivity coefficients accounted for the "thermal imbalance" effect of the backside radiator venting [7]. The total effective solar radiation area was computed based on the spacecraft attitude. Prior to the LOI, the –X-face bus was consolidated with the front-side solar array, which reduced the 8-component spacecraft representation to a 7-component structure. The wider S/C –X plate, as illustrated in Figure 4, can put S/C $\pm Z$ faces in shadow under certain conditions. When the

aspect angle of the Sun and the S/C $-X$ -axis is less than 32° , the S/C $\pm Z$ plates are completely in the shadow. When the angle is greater than 32° , the S/C $\pm Z$ area for solar radiation computation is changing as a function of the aspect angle. To account for this effect, a time-varying Z -area table was generated according to the S/C attitude profile.

To improve the solar radiation modeling, GRAIL conducted a two-week solar calibration for each spacecraft. This activity started immediately after the thruster calibration (early November 2011) and completed a few days before TCM3 (mid-November 2011). Two calibration attitudes, $\pm 45^\circ$ off-Sun, were exercised. Each lasted about one week.

The solar radiation geometry vector can be expressed in equation (1) and its projections along the Sun and the plate normal directions are listed in (2) and (3). As implied in equations (1) – (3), there is no sensitivity in distinguishing the diffuse and specular coefficients when the solar arrays are at the Sun point (i.e. $\alpha = 0^\circ$) attitude. The $\pm 45^\circ$ off-Sun attitudes offer excellent conditions in separating the reflectivity coefficients. With continuous tracking during this period, the navigation team was able to get reasonable estimates of these coefficients and update them prior to the LOI.

$$\vec{F} = F_n \hat{u}_n + F_r \hat{u}_r \tag{1}$$

$$F_n = -a [2\kappa_d v_d + 4\kappa_s v_s \cos(\alpha)] \cos(\alpha) \tag{2}$$

$$F_r = -a [1 - 2\kappa_s v_s] \cos(\alpha) \tag{3}$$

- \vec{F} = the solar pressure geometry vector in a specified coordinate frame
- \hat{u}_n = the unit vector in the direction of the plate normal
- \hat{u}_r = the unit vector from the plate element to the Sun
- a = the plate area
- κ_d = the diffusivity degradation factor, 1 for GRAIL (i.e. assumed no degradation)
- κ_s = the specular degradation factor, 1 for GRAIL (i.e. assumed no degradation)
- v_d = the diffuse reflectivity factor
- v_s = the specular reflectivity factor
- α = the aspect angle of the plate normal and the plate element to the Sun unit vector

3.4. Outgassing

Typically, outgassing events are observed when the spacecraft changes its orientation such that trapped residual material (e.g. water/dry ice, sealants, etc.) is exposed to the Sun. The sublimation and evaporation process causes unwanted gaseous jets that alter the spacecraft flight path. It can take minutes to months for the acceleration to drop to an acceptable level ($< 10^{-12}$ km/s²). The duration of decay depends on the amount and type of residual material left on the spacecraft. There were many GRAIL outgassing events observed during the TLC and Orbital Phases. Figure 7 shows an outgassing example in terms of Doppler pass-through (i.e. predicted or pre-fit) residual. The event involved a first-time S/C Z -face exposure to the Sun. The solved-for (i.e. reconstructed or post-fit) residual, as seen in the example, was fit to the data noise level.

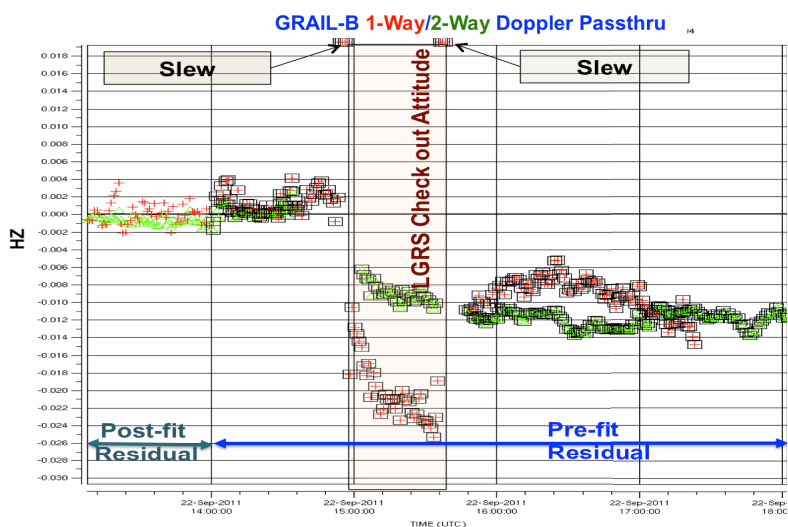


Figure 7: Outgassing Event during LGRS Check Out

When the residual is nearly flat or level, it implies that there are no noticeable dynamic or non-dynamic errors. Vice versa, when the Doppler residual is trending off, there are associated unmodeled errors in the system. Typical non-dynamic errors are media calibrations, station locations, thermal effects (seen in one-way Doppler), etc. Examining the predicted residual in Figure 7, one could easily identify that the residual runoff was not due to non-dynamic errors since the residual was nearly flat before and after the event. This left outgassing as the most plausible explanation for the residual runoff. The sudden shift of the one-way Doppler residual after checkout period was due to the thermal environment changes (a known effect). The total ΔV experienced was ~ 1 mm/s for this particular event.

The associated OD reconstructed outgassing accelerations are shown in Figure 8. As expected, the outgassing acceleration profile resembled an exponential decay signature. A five-minute stochastic batch

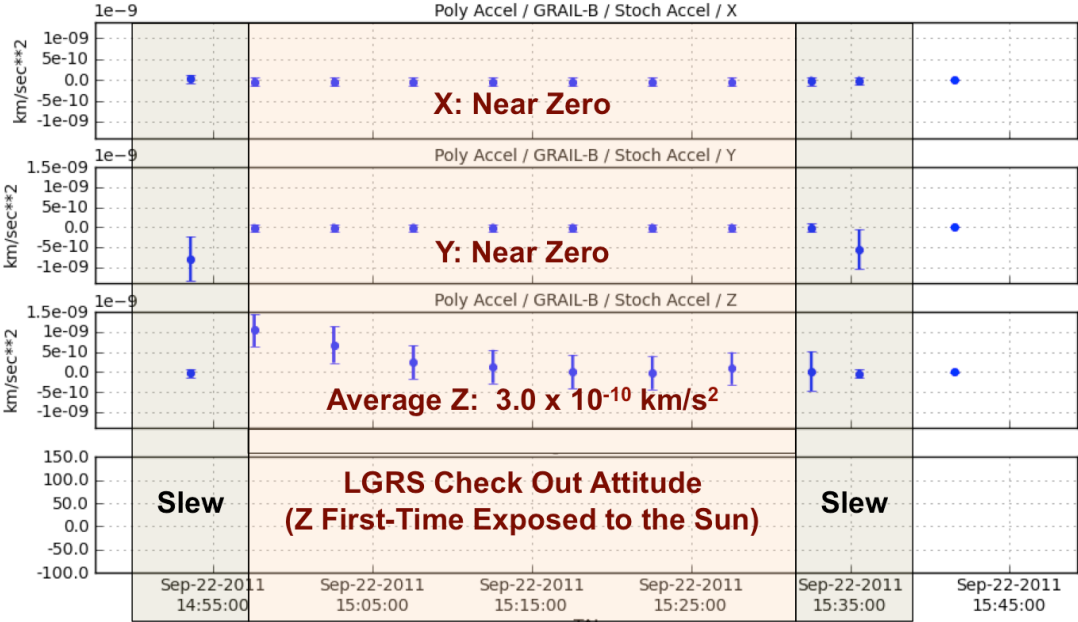


Figure 8: OD Reconstructed Outgassing Accelerations during LGRS Check Out

size was used to reconstruct the event. Since S/C X and Y faces were not exposed to the Sun, the accelerations along these two directions were near zero. The Sun-exposed S/C Z plate experienced an average acceleration of $\sim 3 \times 10^{-10}$ km/s². It was quickly depleted from a peak acceleration of $\sim 1 \times 10^{-9}$ km/s² to an insignificant value in just 20 minutes. Similar phenomena were observed on many other events, such as maneuver slews and spacecraft orientation changes during thruster and solar radiation calibrations. Post-launch orbit determination analysis also uncovered that the outgassing accelerations were decayed to an insignificant level in about two weeks. The accelerations were quickly depleted to a $\sim 10^{-12}$ km/s² level in just a few days after launch. Even though the accumulated ΔV s imparted from the outgassing activities could reach a few mm/s per event, overall they were not significant enough to impact the navigation performance during TLC, LOI, and OPR phases.

3.5. Thruster Events

Maneuver executions were the major thruster events throughout the mission phases. A total of 32 maneuvers were planned for Ebb and Flow to establish the science formation orbit. These maneuvers were the centerpiece of the trajectory designs and implementations. Table 2 summarizes the maneuver timeline and their objectives. There were 15 maneuvers scheduled for GRail-A and 17 for GRail-B. As

indicated in Table 2, five cleanup maneuvers (TCM-A1/B1, TCM-A5/B5, and OTM-B1) were not needed. All the deterministic maneuvers were performed by the main engine. In the pre-launch design,

Table 2: Maneuver Timeline for the Science Orbit Establishment

Maneuver		Epoch	Purpose
TCM-A1/B1		Launch* + 06/07 days	Statistic: Correct injection errors (Canceled)
TCM-A2/B2		Launch* + 20/25 days	Deterministic: LOI Separation
TCM-A3/B3		Launch* + 67/72 days	Deterministic: LOI Target
TCM-A4/B4		LOI – 22/18 days	Deterministic: Combined with TCM3 for LOI target optimization
TCM-A5/B5		LOI – 08 Days	Statistic: Cleanup (Canceled)
LOI	A	31 Dec 2012	Deterministic: Lunar Capture Orbit
	B	01 Jan 2012	
PRM-C1	A1-3	7-9 Jan 2012	Deterministic: Cluster-1, Period Reduction, 1 maneuver per day
	B1-3	13, 15-16 Jan 2012	
PRM-C2	A4-7	24-27 Jan 2012	Deterministic: Cluster-2, Period Reduction, 1 maneuver per day
	B4-7	31 Jan, 1-3 Feb 2012	
TSM	A1	07 Feb 2012	Deterministic: Formation to Science Orbit
	B1	14 Feb 2012	
TSM	A2	20 Feb 2012	Deterministic: Formation to Science Orbit
	B2	24 Feb 2012	
TSM-B3		29 Feb 2012	Deterministic: Science Orbit Finalization
OTM-B1		07 Mar 2012	Statistic: Cleanup (Canceled)

* Launch Time - 10 Sep 2012 13:08 UTC

TCM-4A/4B were supposed to be implemented as statistical maneuvers for cleaning up the LOI targeting errors. During flight operation, the navigation team combined TCM-3 and TCM-4 in the design process. The dual-TCM optimization proved to be a better LOI targeting strategy.

Besides maneuver executions, small forces induced by RWA desaturation activities were thought to be an influential source of trajectory perturbations in flight, especially during the Primary Science phase. By design, the coupled ACS thrusters were not supposed to impart net translational ΔV s to the system. In reality, since no thruster was built and configured exactly according to the blueprint, misalignments and other factors could impact the balanced system. To assess the impacts of these unwanted ΔV s, a thruster calibration took place at the beginning of November 2011 on each spacecraft. The main objective of the thruster calibration was to characterize the thruster direction and impulse-bit output. Reconstructed knowledge obtained through filtering and trending

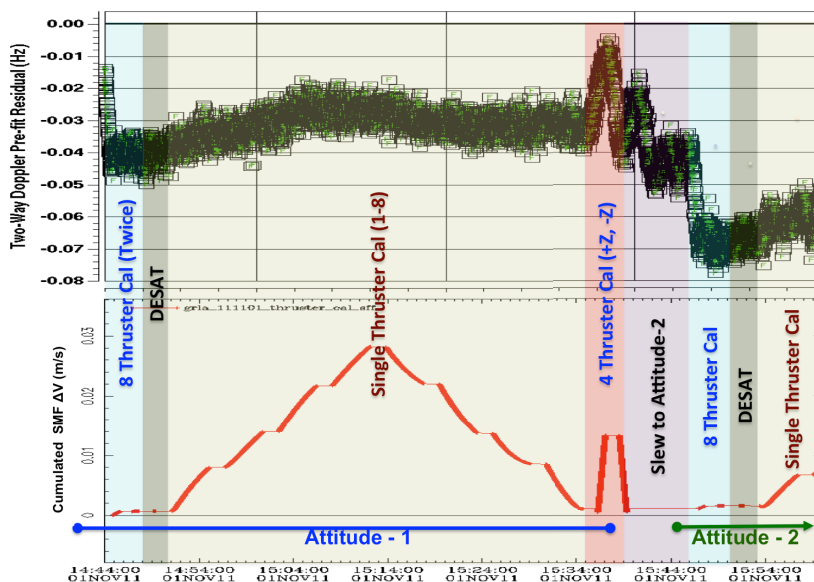


Figure 9: Thruster Calibration Attitude – 1: Pre-fit Residual with On-board Reconstructed SMF, GRAIL-A

analyses was used to update the onboard ACS control parameters and ground tools.

Three mutually orthogonal attitudes were carefully selected such that each thruster direction and magnitude could be reconstructed with Doppler and the on-board telemetry information. It took about three hours to complete the entire calibration sequence. Each attitude consisted of three different thruster combinations: 1) activating all 8 thrusters simultaneously for 40 seconds; repeat once; 2) activating each thruster individually for 160 pulses (60 milliseconds/pulse, 1.5 seconds off time before initiating the next thruster); 3) activating 4-thruster combination at a time to first generate +Z ΔV and then -Z ΔV . The single thruster firing sequence was arranged specifically to minimize the ΔV impact to the system.

Figure 9 demonstrates the entire attitude-1 thruster firing sequence and attitude-2 partial sequence. The cumulated ΔV was directly plotted from the on-board reconstructed small force (SMF) data, which were based on the thruster impulse-bit (I_{bit}) equation with inputs from telemetry information. In Figure 9, the net ΔV from the 1st time 8-thruster firing was not the same as the 2nd time 8-thruster firing. In theory, they both should be zero. The corresponding two-way S-band Doppler residual shows that the on-board reconstructed ΔV from the first 8-thruster firing had about 2 mm/s line-of-sight (LOS) error while the second 8-thruster firing had nearly zero LOS error. This implies that the I_{bit} equation yielded a much better estimate when thruster outputs were in a steady state. From Figure 10, the OD reconstructed solution shows that the first time 8-thruster firing had a much bigger correction than others. The corresponding Doppler residual shows that the

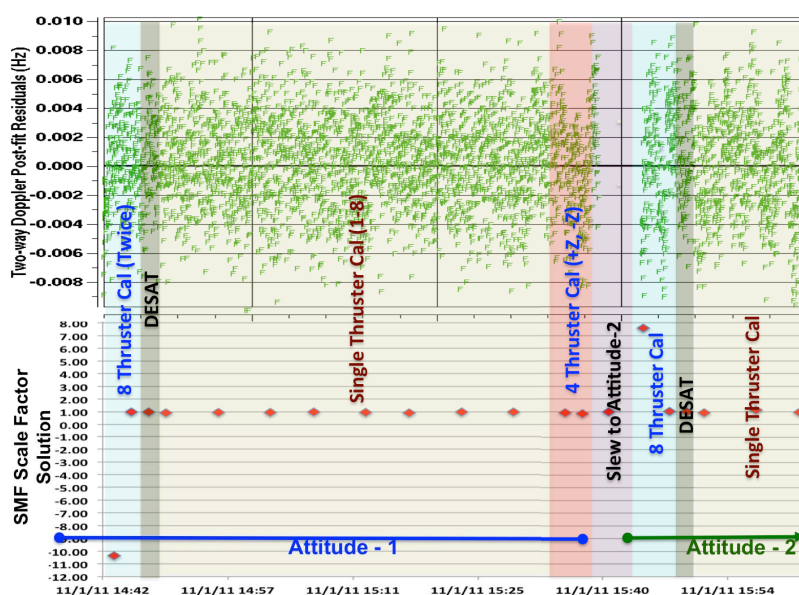


Figure 10: Thruster Calibration Attitude – 1: Post-fit Residual

on-board reconstruction had a small ~ 0.2 mm/s LOS error; that is, there are no noticeable misalignment problems. The 4-thruster set firings further proved that the ACS system performed nominally in a steady-state environment.

4. Orbit Determination Configuration

The JPL “Mission-analysis, Operations, and Navigation Toolkit Environment” (MONTE) software set was used to perform navigation functions, including orbit determination. The OD major capabilities include:

- 1) Obtaining the Spacecraft Trajectory Current-State Knowledge: This is done by estimating the spacecraft state via minimizing tracking data residuals through a linearized filter. In addition to the S/C state, refined dynamic parameters, such as solar radiation parameters and thruster events, are usually estimated or considered;
- 2) Capturing Statistics for Current and/or Future Trajectory Events: Filtered statistics along with future error assumptions (including dynamic and non-dynamic noise or biases) are mapped to

interested trajectory events, for instance, current maneuver execution statistics, future apses events, etc.

- 3) Trending and Improving Spacecraft Dynamics for Long-Term Propagation: This is an important function in terms of supporting trajectory designs and implementations. The estimated parameters often only represent local corrections or knowledge. To do a better job, OD analysts are required to take the local information and trend it with other known long-term environmental factors to attain a global knowledge of a particular dynamic model. This process is sometimes open ended; that is, the model is always adjusted and refined. A good example is small force trending.

The GRAIL real-time OD process typically takes about 4 hours to complete. Figure 11 illustrates a simplified OD process. Typical external interfaces consist of tracking data, reconstructed and/or planned thruster activities, S/C orientation changes, and media corrections. Updating these inputs takes about an hour of preparation time. It usually takes about 2 hours to perform the orbit determination itself including refining the filter strategy and validating the tracking data and models. It depends on the mission phase and propagation end time. The product generation can be time consuming. For example, propagating a two-week trajectory with a full-field lunar gravity in a two-hour orbit can take quite a bit of CPU time.

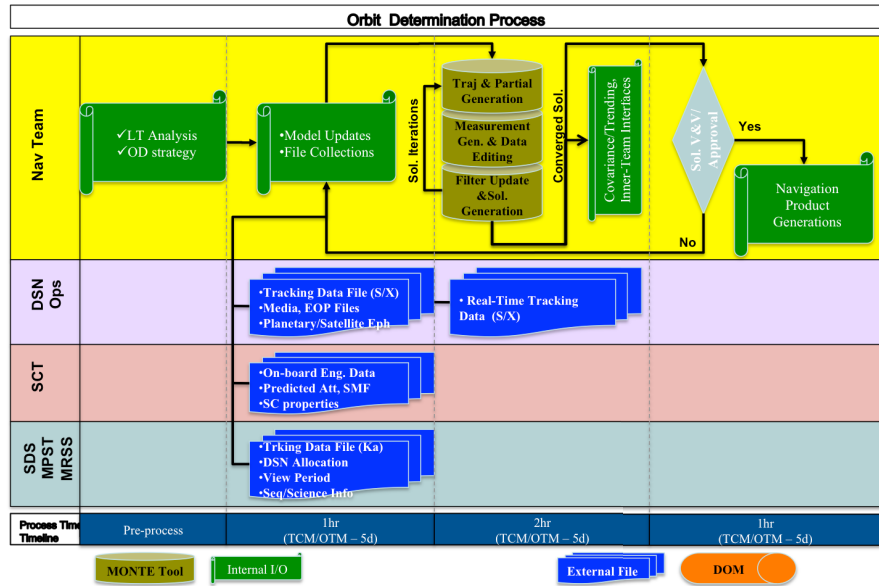


Figure 11: GRAIL Orbit Determination Process

4.1. Tracking Data

The S-band two-way Doppler and two-way range (TLC phase only) are the standard data types used in OD solutions. Most of time, the USO enabled one-way X-band Doppler was not included in the solutions, which was contrary to the original plan. It was thought to be an excellent complimentary data source to enhance the navigation performance pre-launch; however, due to thermal fluctuation caused by heater cycling, it prevented navigation from using this data type during the flight operation. Figure 12 shows how heater cycling corrupts the USO X-band data. The purpose of cycling on and off was to maintain the subsystem temperature profile. Although the USO X-band one-way Doppler was corrupted in the early mission phases, it has stabilized and presently

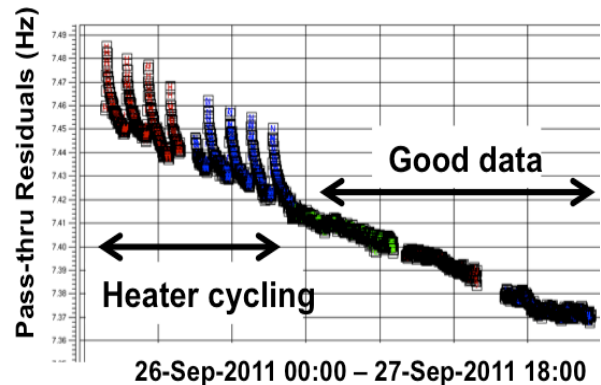


Figure 12: X-band One-way Doppler

serves as a good source for solution validation.

Corrupted tracking signals were also found in two-way Doppler during OPR/TSF phases. A combination of the low periapsis altitude, spacecraft attitude (recall Figure 6, 40° off Sun-pointing), and orbit geometry made transmitting signals bounce off from a direct-Earth path to a lunar-surface multipath route before reaching the ground receiver. These data were not usable for OD and imposed a challenge in separating these corrupted data from other dynamic mismodeling signatures (e.g. gravity error). Figure 13 demonstrates pass-through residual of corrupted tracking data (square boxes inside the highlight areas). OD analysts often had to process a small set of data to get the dynamic signatures down to a certain level and then used the pass-through technique to eliminate the corrupted data.

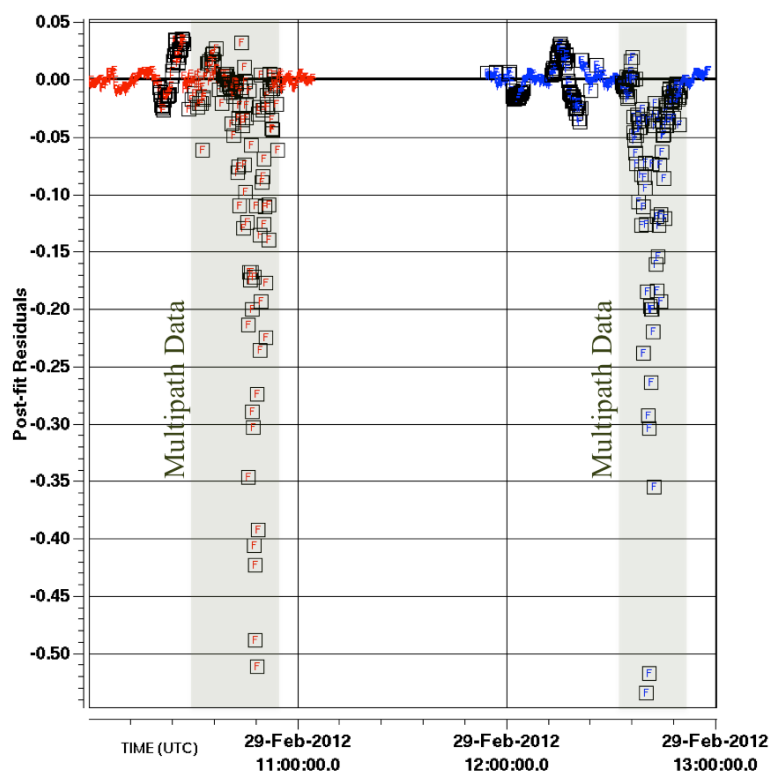


Figure 13: Corrupted Multipath Tracking Data

GRAIL relied on the NASA Deep Space Network (DSN) for tracking and communication. Antennas at Goldstone in California, Madrid in Spain, and Canberra in Australia participated in tracking GRAIL. DSN range data are represented as “range unit”, or RU. At GRAIL’s S-band frequency, 1 RU is equal to ~ 0.145 meter. As shown in Table 3, GRAIL was tracked extensively during launch, LOI, and in-orbit phases. Range data were available all the way to lunar capture.

Table 3: DSN Tracking Data Coverage prior to the Science Phase

Mission Phase	Key Events	Begin	End	Doppler Range (before LOI)	Remark
Launch	TCM-1 (A/B)	L + 000d	L + 015d/020d	Continuous	Dual complex during Launch
Trans-Lunar Cruise	TCM2-5 (A/B)	L + 015d/020d	LOI – 008d	1 pass/2day	8 hr/pass per S/C
	TCM Design	TCM – 006d	TCM – 005d	2-3 pass/day	~16 hr/day
	TCM Execution	TCM – 002d	TCM + 002d	Continuous	
Lunar Orbit Insertion	LOI	LOI-A – 008d	LOI-B + 001d	Continuous	Dual complex during LOI
Orbit Period Reduction	PRMC1 (A/B)	LOI-B + 001d	12/18 Jan’12	Continuous	Some small gaps
	PRMC2 (A/B)	12/18 Jan’12	05 Feb’12	2-3 pass/day	~16 hr/day
Transition to Science Formation	TSM1-2	05 Feb’12	22 Feb’12	2-3 pass/day	~16 hr/day
	TSMB3 OTMB1	22 Feb’12	07 Mar’12	Continuous	

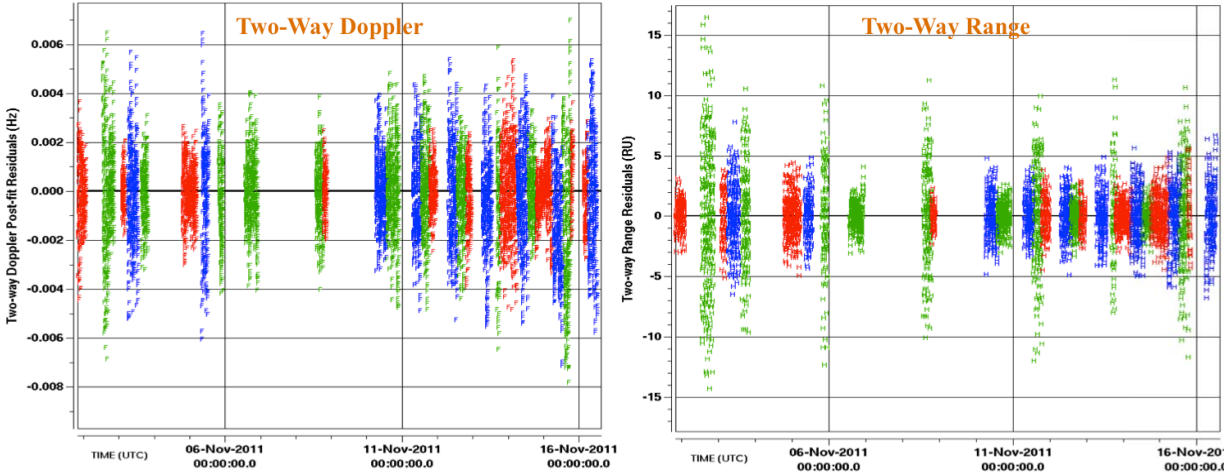


Figure 14: Two-way Doppler and Range Data Quality

The in-flight observed tracking data accuracy was much better than the pre-launch expectations. Figure 14 shows the mid-cruise post-fit residuals of GRAIL-A’s two-way S-band Doppler and range data. The associated Doppler and range standard deviations were 0.0018 Hz and 2.6 range unit (RU). Table 4 summarizes the expected and in-flight observed tracking accuracy in the metric system. The actual performance was about 6 times better than the pre-launch assumptions.

Table 4: Pre-launch and Observed Tracking Noise (S-Band)

Data Type	Pre-launch Assumption (1σ)	Observed (1σ)	Remark
Two-way Doppler	1 mm/s	0.10 - 0.15 mm/s	60 second sampling 1 mm/s \approx 0.015 Hz
Two-way Range	3 m	\sim 0.5 m	1 m \approx 7 RU

4.2. Filter Configuration

4.2.1 Trans-Lunar Phase Filter

The GRAIL TLC baseline filter strategy was configured based on in-flight experiences. It deviated slightly from the pre-launch assumptions. Noticeably, a 50 RU (\sim 7.2 m) range bias per station was added in the filter to account for an unknown error at the time. This was additional to the pre-launch configuration, which included a 21 RU (\sim 3m) range bias per pass. The introduction of this bias was to deal with an uncharacterized error at Deep Space Station 45 (DSS-45). Figure 15 clearly shows that DSS-45 had an out-of-family bias with respect to the rest of stations. Later in the flight, it was identified to be an error in calibrating the antenna Z-height at that station.

Another key update was the tracking data-weight strategy. Starting mid-TLC, GRAIL adopted an automatic data editing and weight strategy. The auto-

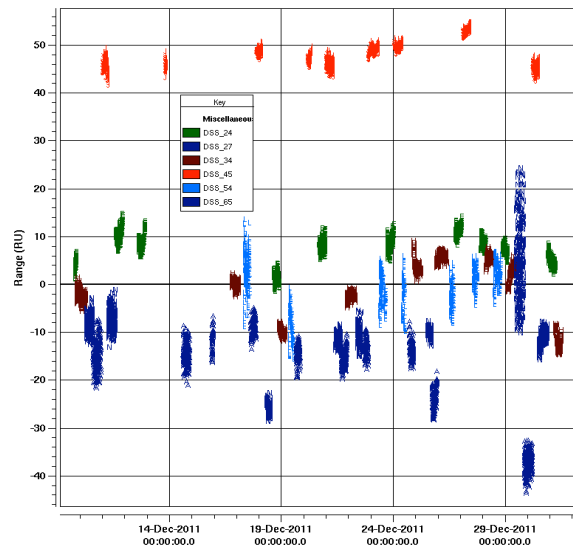


Figure 15: Unexpected DSS-45 Range Bias, RU

editor detected blunder points based on preset criteria and the auto-weight computed the per-pass noise automatically. To account for the Doppler noise from the interplanetary solar plasma effect, a de-weighting scale factor (~3.4) was applied to the computed per-pass noise. There were floor values for this auto-weighting scheme: range was set at 7 RU and Doppler at 0.0015 Hz. Setting a minimum threshold was necessary to protect the possibility of over-weighting some particular passes.

Compared with the pre-launch configuration, a few small but important in-flight updates were made: 1) changing the non-gravitation noise to a non-spherical error model; 2) reducing the future non-gravitation noise to about 40% level; 3) in conjunction with the thruster location configuration, computing RWA desaturation *a priori* sigma automatically from the downlinked telemetry thruster counts and on-times with an assumption of a 10% unbalanced system; 4) reducing the TCM fixed magnitude error to 1 mm/s from 7 mm/s for TCM-4 and TCM-5; 5) estimating media corrections instead of treating them as “consider” parameters.

Maintaining a consistent baseline filter strategy serves as an essential role in evaluating OD solutions. Like many other systems, when dealing with future uncertainties, there are built-in margins to account for unknown or uncharacterized perturbations. To gauge an “irreducible minimum perturbation” scenario, a “No Margin” filter configuration was created. This helped the project to understand the “bare bones” solutions and the associated implications. Table 5 summarizes the baseline and “No Margin” filter configurations. The “No Margin” filter setup was heavily constrained with respect to estimating solar radiation parameters, momentum desaturations, and non-gravitational forces. The *a priori* uncertainties were based on historical dynamic trending analysis.

Table 5: In-flight Trans-lunar Cruise OD Filter Configuration

Error Source	Estimate Type	Baseline	No Margin		Correlation Time	Update Time	Comments
		A Priori Uncertainty (1σ)	A Priori Uncertainty (1σ)				
S-Band 2-way Doppler (hz)	–	per pass	per pass				floor at 0.0015 hz
S-Band Range (RU)	–	per pass	per pass				floor at 7 RU / 4 RU
Epoch state position (km)	Estimate	100000	100000				Earth, Sun or Moon-Centered ICRF Cartesian
Epoch state velocity (km/s)	Estimate	10	10				
Solar Radiation Pressure Coefficient (% of total)	Estimate	20	5				flat plate component model
Range Bias (RU)	Estimate	50	50				Per station bias
		21	21			per pass	stochastic
Ionosphere – day / night (cm)	Estimate	20	20	white		per pass	stochastic
Troposphere – wet / dry (cm)	Estimate	2	2	white		per pass	stochastic
AMD Event ΔV (mm/s)	Estimate	Various	0.5 mm/s			per event	per axis
Solar Cal Constant Acceleration (km/s ²)	Estimate	5.00E-12	5.00E-12	white		during event time	per axis constant bias
Non-Grav Acceleration (km/s ²)	Estimate	5.0e-12 / 2.0e-12 / 2.0e-12	2.0e-12 / 2.0e-12 / 2.0e-12	white		per day	stochastic
Future Acceleration (km/s ²)	Estimate	2.00E-12	5.00E-13	white			per axis stochastic; 1.0E-11 during early TLC
Earth–Moon Ephemeris	Consider	DE421 Covariance	DE421 Covariance				~4 m lunar position error at time of Mission
Earth GM (km ³ /s ²)	Consider	1.40E-03	1.40E-03				
Moon GM (km ³ /s ²)	Consider	1.00E-04	1.00E-04				
Station Locations (km, deg, km)	Consider	Covariance	Covariance				
Pole X, Y (cm)	Consider	10.0 / 10.0	10.0 / 10.0				1.5e-08 radians
UT1 (cm)	Consider	10	10				0.3e-03 seconds
Maneuver Execution Errors (3σ)	Estimate Type	Based on Model	ΔV magnitude		Pointing		Comments
			Fixed	Proportional	Fixed per axis	Proportional Total	
TCM-1 (Canceled)	Estimate	ME Pre-Crosstrack Calibration	7 mm/s	0.25%	3 mm/s	(-4/15)* DV +6+5/15)% for 5<DV<20 m/s	Force, Pointing (RA, Dec)
TCM-2 - TCM-3	Estimate	ME Translational-Crosstrack Calibration	7 mm/s	0.25%	1 mm/s	1.00%	Force, Pointing (RA, Dec)
TCM-4 – TCM-5* (TCM-5 Canceled)	Estimate	ME Duty Cycle	1 mm/s	1.67%	1 mm/s	0.60%	Force, Pointing (RA, Dec)

4.2.2 In-Orbit Filter

Once GRAIL achieved lunar orbit, the OD filter strategy was simplified. Table 6 lists the baseline in-orbit filter configuration. The ranging system was turned off. The non-gravitation accelerations were also removed. Compared with the cruise phase, the *a priori* uncertainties of the S/C state were constrained significantly. The solar pressure parameter was tightened down to a 5% level (1σ). The consider parameters, RWA desaturations, media corrections, and data auto-weighting scheme were unchanged.

Table 6: In-orbit OD Filter Configuration

Error Source	Estimate Type	Baseline			Comments		
		A Priori Uncertainty (1σ)	Correlation Time	Update Time			
S-Band 2-way Doppler (hz)	–	per pass			floor at 0.0015 hz		
Epoch state position (km)	Estimate	1000			Earth, Sun or Moon-Centered		
Epoch state velocity (km/s)	Estimate	1			ICRF Cartesian		
Solar Radiation Pressure Coefficient (% of total)	Estimate	5			flat plate component model		
Ionosphere – day / night (cm)	Estimate	20	white	per pass	stochastic		
Troposphere – wet / dry (cm)	Estimate	2	white	per pass	stochastic		
AMD Event ΔV (mm/s)	Estimate	Various		per event	per axis		
Preiapsis Absorber (mm/s)	Estimate	Various			2-5 mm/s typically		
Future Acceleration (km/s ²)	Estimate	Various (Periodical)	white		stochastic; to account for gravity errors		
Earth–Moon Ephemeris	Consider	DE421 Covariance			~4 m lunar position error at time of Mission		
Earth GM (km ² /s ²)	Consider	1.40E-03					
Moon GM (km ² /s ²)	Consider	1.00E-04					
Station Locations (km, deg, km)	Consider	Covariance					
Pole X, Y (cm)	Consider	10.0 / 10.0			1.5e-08 radians		
UT1 (cm)	Consider	10			0.3e-03 seconds		
Maneuver Execution Errors (3σ)	Estimate Type	Based on Model	ΔV magnitude		Pointing		Comments
			Fixed	Proportional	Fixed per axis	Proportional Total	
LOI, PRMs, TSMs	Estimate	Based ME Burn	7 mm/s	0.25%	1mm/s	0.50%	Force, Pointing (RA, Dec)

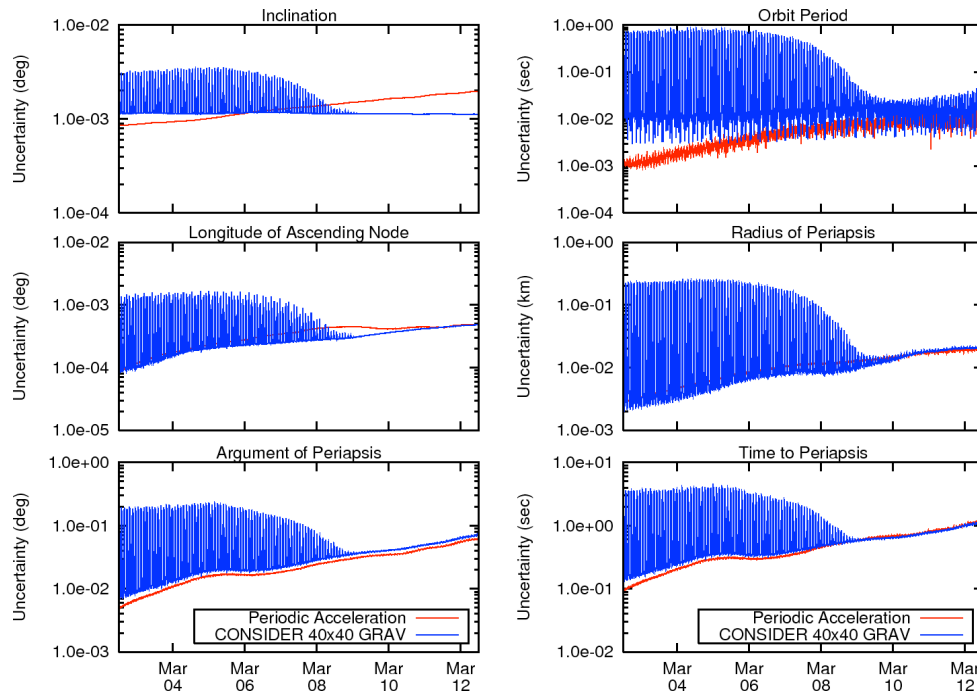


Figure 16: Considering a 40x40 gravity Covariance vs. Periodic Acceleration Model

Pre-launch statistical analysis used a subset of the LP150Q covariance (i.e. 40x40) to validate the navigation requirements; however considering a 40x40 gravity covariance to get future event statistics was quite time consuming. This approach was impractical in operation. To simulate the gravity error, periodical accelerations were introduced. The advantage of this approach was the run-time savings. A parametric analysis was performed to approximate the orbit element errors. By selecting appropriate periodic terms and focusing on the key elements impacting the navigation requirements, a representative set of parameters was chosen to replace the gravity covariance. The key elements to monitor were inclination, longitude of ascending node, separation distance, and time to periapsis. As shown in Figure 16, the periodic approach was in reasonable agreement with the gravity covariance run. OD errors in radius of periapsis and argument of periapsis were not driving the design. In short, considering the periodic acceleration error model in the OD filter was a good alternative to considering the lunar gravity covariance. This process was updated periodically as the orbit changed in flight.

5. Orbit Determination Evaluations

5.1. Launch Vehicle Performance

Approximately two and half an hour after the Launch (L), the GRAIL navigation team received two-way Doppler data from the DSN Goldstone station. The first priority for the OD team was to perform quick turn-around solutions and support the second station rise at Canberra, Australia, which was in-view at about L+8.5hr. The OD analysts delivered their first GRAIL-A and GRAIL-B solutions at L+7hr as planned with five and half an hours of Goldstone two-way Doppler. These solutions were used to update the ground antenna predictions. Subsequent solutions at L+14hr, L+1day, and L+2day were delivered to the project and DSN for trajectory analysis and predict updates.

A simple current-state estimation strategy was adopted for these early solutions since the data-

Table 7: LV Target Performance Evaluated at Target Intercept Point (TIP)

Parameter	L.V. Target	OD Reconstructed	Error (σ)
C_3 (km^2/s^2)	-0.696	-0.693	0.24
Eccentricity DEC (deg)	-6.160	-6.164	0.32
Eccentricity RA (deg)	190.543	190.548	0.28

arc was too short to sense the long-term dynamic trends. Also, the requirements to

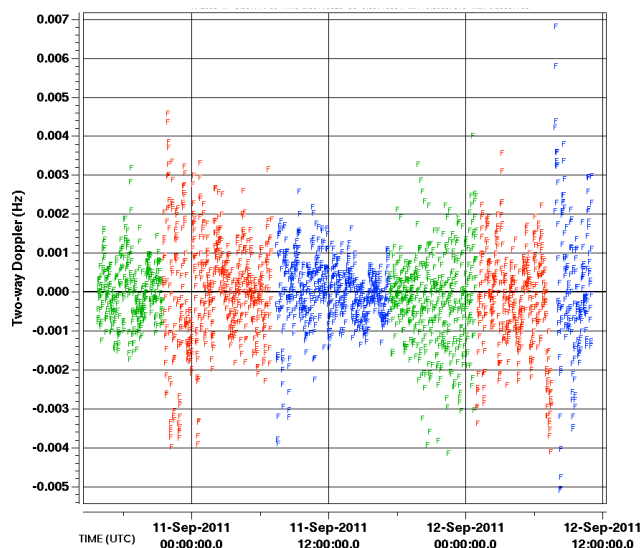


Figure 17: Doppler Residual at L+48hr Solution

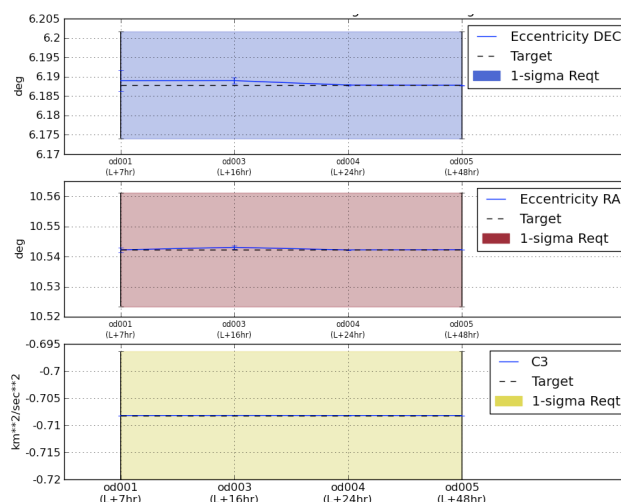


Figure 18: LV Performance Evaluated at L+7hr

support the DSN acquisitions were loose enough to ignore the long-term dynamic errors. Evaluations based on the OD reconstructed solutions revealed that the Launch Vehicle (LV) performance was superb, which was well within 1-sigma of the pre-launch expectation. Table 7 shows the launch vehicle performance at the Target Intercept Point (TIP) using the L+48hr OD solution. Since the data arc started much later than the TIP epoch, the solution was integrated backward to get the reconstructed TIP state and the corresponding uncertainties. As shown in Figure 17, continuous two-way Doppler data from three DSN complexes were included in this solution. The multi-complex tracking data helped to clamp down the orbit uncertainty at the event time of interest. Figure 18 compares OD solutions with the nominal launch trajectory mapped to L+7hr. It further confirmed that the LV performance was remarkably good.

5.2. Trans-Lunar Cruise Solution Evaluation

During cruise, the OD team concentrated on validating the tracking data, analyzing spacecraft dynamics, and performing orbit determination. Key dynamic analyses are discussed in Section III. Tracking data

analyses are also briefly summarized in Section IV. The focus of this section is to discuss methods of solution evaluations.

As mentioned in Section II-B, since GRAIL was not on a hyperbolic trajectory, solution evaluation in a B-plane system was not available. Instead, the OD team created a pseudo B-plane or LOI-plane (also known as an “Egg” plot for its resemblances to an open-faced egg).

To define the LOI-plane, let $Y_r(t)$ be the unit vector parallel to the Moon’s velocity relative to the Earth at time t and $\phi_r(t)$ be the unit vector along the instantaneous spin pole of the Moon such that $X_r(t) = (Y_r(t) \times \phi_r(t)) / \|Y_r(t) \times \phi_r(t)\|$ and $Z_r(t) = X_r(t) \times Y_r(t)$. The LOI-plane coordinates X , Y , and Z are inertially fixed and defined by $X_r(t_{cross})$, $Y_r(t_{cross})$, and $Z_r(t_{cross})$, respectively, where t_{cross} is the epoch when the nominal trajectory for GRAIL-A or GRAIL-B crosses the $X_r(t) -- Z_r(t)$ plane. Note that X , Y , and Z are slightly different directions for GRAIL-A and GRAIL-B. Figure 19 illustrates the LOI-plane. The sub-plot represents the solution lunar-encounter times and the associated uncertainties with respect to the target time. A timing threshold (blue band), as shown in Figure 19, was defined to monitor solutions. Figure 20 shows solutions at a closer scale. The blue band represents the safe-zone threshold corresponding to the encounter

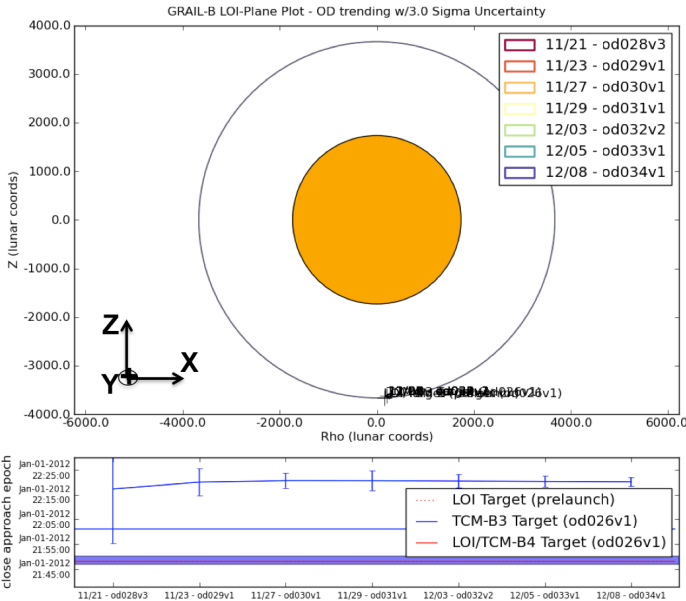


Figure 19: Pseudo B-Plane Plot

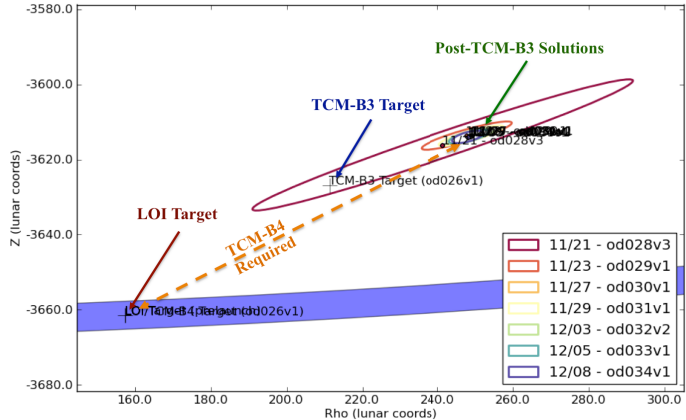


Figure 20: Zoomed-in Solutions

lunar radius. To satisfy the post-LOI orbit condition, both target time and encounter lunar radius need to be within the pre-defined thresholds. These thresholds were loosely defined based on pre-launch TCM4 covariance analysis and were replaced by a more stringent criteria post-TCM4.

As the mission progressed, a more disciplined approach was adopted to determine the TCM5 Go/No-Go criteria. Recall that TCM3 and TCM4 were combined in the LOI-target optimization, this left TCM5 the only statistical maneuver before LOI. To determine whether a “Go” or “No Go” decision on TCM5, the navigation team created a “safe-zone” box based on Monte Carlo trajectory analysis³. This “safe-zone” box was constructed with “LOI-Target Timing Error” as the x-axis and “LOI Radius” as the y-axis.

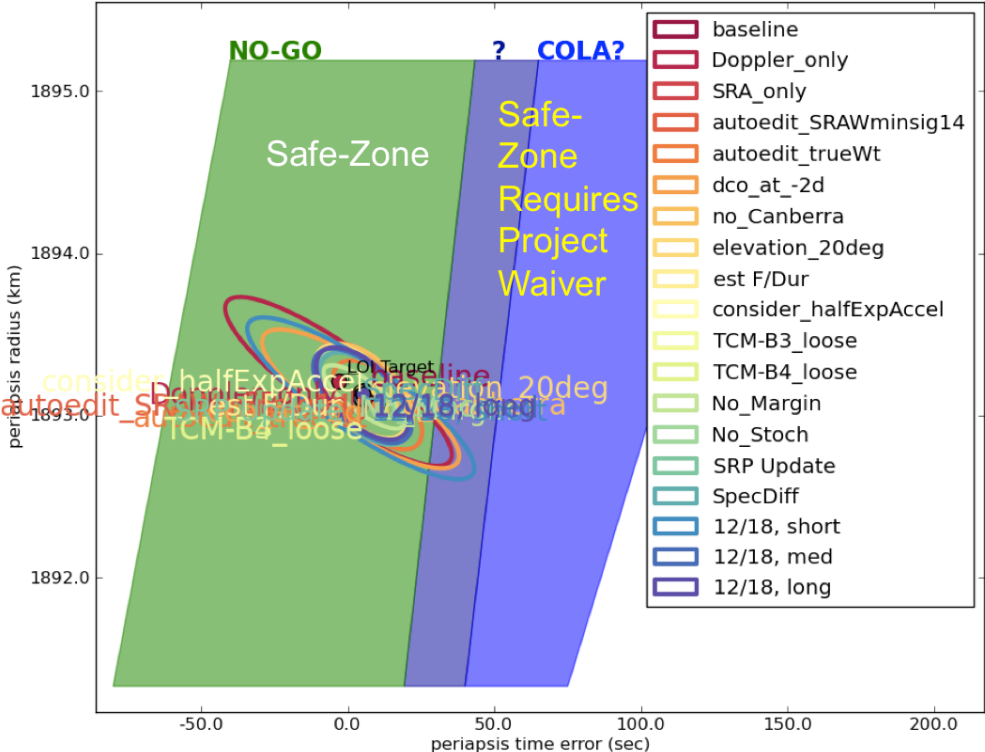


Figure 21: Post-TCM-4B Filterloop Solutions, 3σ

As shown in Figure 21, the “NO-GO” zone was designated as an absolute “Safe Zone”. As long as solutions were bounded within this green box, it was a “No-Go” for TCM5. For solutions falling onto the other color zones (i.e. blue and grey-blue zones), the decisions were at the project’s discretion. For solutions within these bluish zones, the orbiters might have a slight chance to encounter a collision avoidance (COLA) issue in a later orbital phase. Since COLA was not difficult to mitigate and the probability for it to occur was extremely small, these zones served more as a precautionary step in preventing an unwanted scenario.

Along with nominal solutions, a series of filter variations (filterloop) were constructed for “blind-spot” checks. These filterloop solutions included the no margin case, data weight and editing variations, dynamic sensitivities, data arc and data cutoff scenarios, and tracking data types and DSN station alternations. As illustrated in Figure 21, these solutions were tightly grouped around the LOI-B target. Results from these “blind-spot” checks suggested a “No-Go” for TCM-B5. Similar analysis was performed on GRAIL-A and the conclusion was to cancel TCM-A5 as well.

5.3. Maneuver Estimation

GRAIL maneuvers were executed in a blow-down mode; therefore the force model could not be easily expressed with a simple constant model. In operation, a six-degree polynomial was generated to represent the expected thrust curve for each maneuver. With these polynomial coefficients incorporated in a burn model, the OD team then was able to baseline a maneuver estimation strategy. Along with the thrust direction and the total burn duration, the force could be estimated as constant, linear, or quadratic terms (i.e. F_0, F_1, F_2). The objective of maneuver reconstructions was to accrue the knowledge of maneuver estimations and to improve the maneuver execution performance. Figure 22 shows an example of estimated force models comparing with predicted models for a particular maneuver. As seen in the figure, the signature of the predicted polynomial force model (denoted as “Poly-Force Model”) was quite different from the on-board reconstructed force model. Since the shapes and signatures were noticeably incompatible between the predicted and actual models, it caused great difficulty when fitting the data. This became even more evident during low-altitude and near-circular orbit phases due to significant interference from the lunar gravity error. To mitigate this problem, shortening the post-burn data arc and constraining the epoch state was found to be a good approach. The disadvantage was slightly larger posterior uncertainties. Other force models were also investigated, for instance, linear model and multi-finite burn model. Some cases did promote the post-fit residuals, however the improvement was not seemingly clear in terms of burn direction estimates. As demonstrated in Figure 23, the maneuver execution errors from linear and polynomial force models were almost identical.

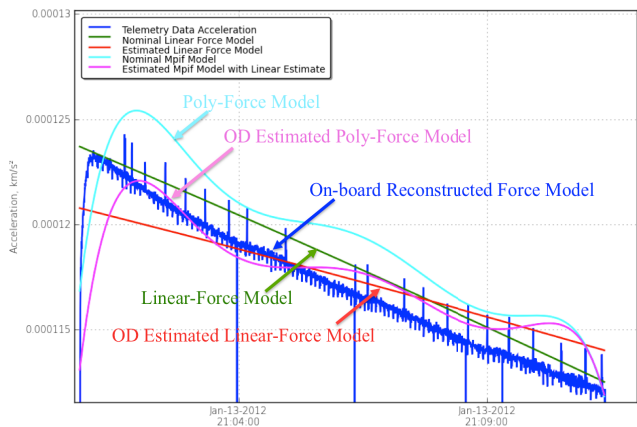


Figure 22: Estimated Maneuver Force Models

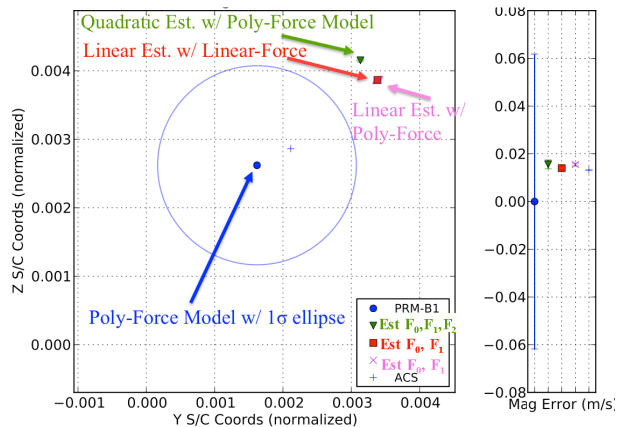


Figure 23: Maneuver Execution Error

The navigation team also invested a special effort in implementing and configuring the real-time Doppler residual display to monitor maneuver executions. This gave first-hand information to the project and navigators in assessing burn performance in real-time. In case of a S/C anomaly, it also could provide an early warning signal to the flight system for appropriate contingency responses. Figure 24 shows an

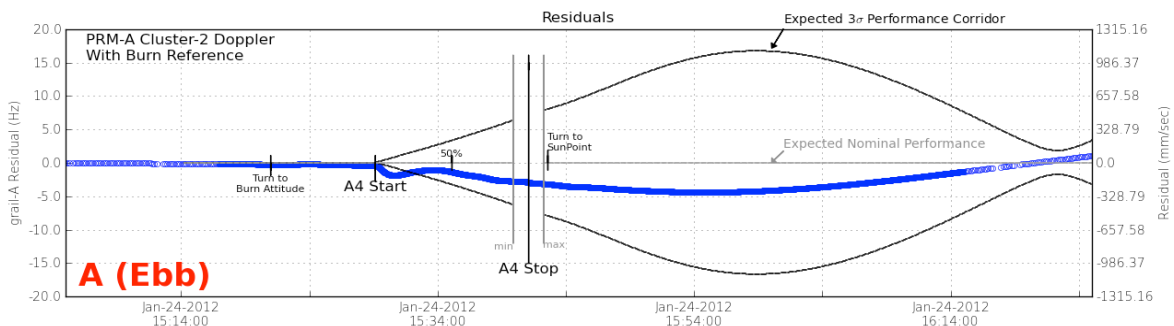


Figure 24: Real-Time Display Monitoring PRM-A4

example of the Real-Time Display during PRM-A4, which indicated a nominal performance (i.e. the post-burn residual was well within the 3σ expectation).

6. Conclusion

After successfully executing 27 maneuvers on their six-month journey, Ebb and Flow established the most stringent planetary formation orbit on 29 February 2012. A total of five statistical maneuvers, two from Ebb and three from Flow, were eliminated because of outstanding performance from launch vehicle, flight operation, and navigation systems. The Science Phase started a week earlier than planned. As shown in Figure 25, the relative orbital element differences between Ebb and Flow after reaching formation were well within the requirements [8]. The GRAIL project met its minimum mission success criteria at the midpoint of the Primary Science Phase. As of today, including science data collected from the extended mission, five science cycles have been completed. Together, they have made an unprecedented achievement in the lunar science community.

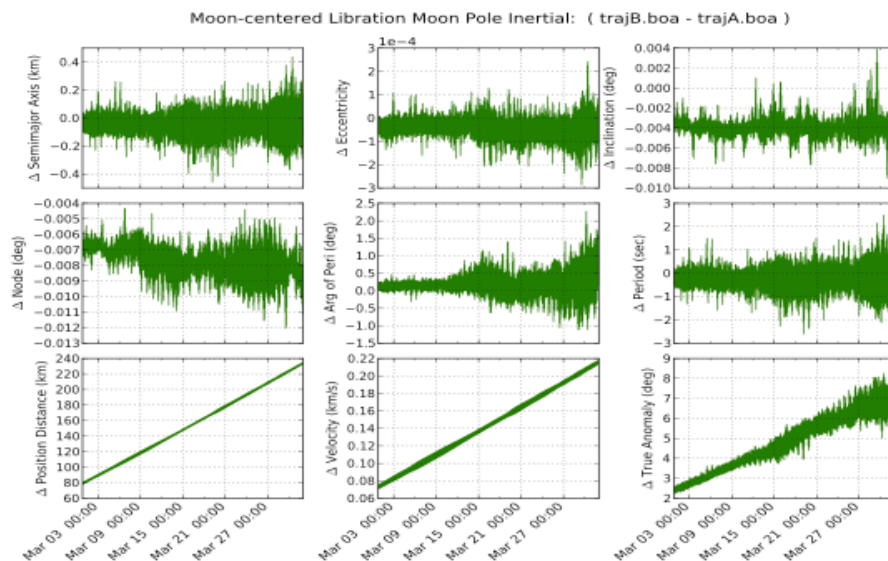


Figure 25: GRAIL-A and GRAIL-B Orbit Differences after Formation Orbit Achieved

This paper compiles the orbit determination strategy, process, and experiences in meeting the project requirements. GRAIL is the first mission to generate a full high-resolution gravity field of the only natural satellite of the Earth. It not only enables scientists to understand the detailed interior structure of the Moon but also further extends their knowledge of the evolutionary histories of the rocky inner planets. Robust and successful navigation was the key to making this a reality.

Acknowledgments

This work was carried out at the Jet Propulsion Laboratory, California Institute of Technology, Pasadena, California under contract to the National Aeronautics and Space Administration. The authors would like to thank the support of GRAIL Project, Lockheed-Martin Space Systems, and JPL DSN Operation, and Mission Design & Navigation Section.

7. References

- [1] Roncoli, R. B. and Fujii K. K., “Mission Design Overview for the Gravity Recovery and Interior Laboratory (GRAIL) Mission”, AIAA 2010-8383, Toronto, Ontario Canada, 2010.
- [2] Chung M. J., et al., “Trans-Lunar Cruise Trajectory Design of GRAIL (Gravity Recovery and Interior Laboratory Mission)”, AIAA 2010-8384, Toronto, Ontario Canada, 2010.
- [3] Antreasian P., et al., “Navigation of the Twin GRAIL Spacecraft into Science Formation at the Moon”, 23rd International Symposium on Space Flight Dynamics, Pasadena, California, 2012.
- [4] Tapley, B., et al., "GGM02 - An improved Earth gravity field model from GRACE", Journal of Geodesy, 2005, DOI 10.1007/s00190-005-0480-z.
- [5] Konopliv, A.S., et al., “Recent Gravity Models as a Result of the Lunar Prospector Mission”, 150, Issue 1, March 2001, pp. 1–18. (available online at <http://www.idealibrary.com>).
- [6] Folkner, W. M. , J. G. Williams, D. W. Boggs, “Planetary Ephemeris DE421 for Phoenix Navigation,” JPL IOM 343R-08-002, Feb. 13, 2008.
- [7] You, T. H., et al., “Mars Reconnaissance Orbiter Interplanetary Cruise Navigation”, 20th International Symposium on Space Flight Dynamics, Annapolis, Maryland USA, 24-28 September 2007.
- [8] Hatch, S. J., et al., “GRAIL Trajectory Design: Lunar Orbit Insertion through Science”, AIAA 2010-8385, Toronto, Ontario Canada, 2010.